

# ACHIEVABLE ORBIT ESTIMATION ACCURACY THROUGH SPACE-BASED PASSIVE OPTICAL OBSERVATIONS: A SENSOR REQUIREMENT ANALYSIS

Felix Stechowsky<sup>(1)</sup>, Srinivas Setty<sup>(2)</sup>, and Alejandro Pastor<sup>(3)</sup>

<sup>(1)</sup>Technical University of Darmstadt, Karolinenplatz 5, 64289 Darmstadt, Germany, Email: felix.stechowsky@web.de

<sup>(2)</sup>GMV, Friedrichshafener Straße 7, 82205 Gilching, Germany, Email: ssetty@gmv.com

<sup>(3)</sup>GMV, Calle Isaac Newton 11, Tres Cantos, 28670, Spain, Email: apastor@gmv.com

## ABSTRACT

This work investigates the potential of space-based optical observations for orbit determination and the achievable estimation accuracy. The objective is to contribute to the definition of guidelines and requirements for the development of future space-based sensor systems, which will enhance Space Surveillance and Tracking (SST) capabilities. In particular, the impact of measurement noise and position uncertainty of the observing satellite on the orbit estimation accuracy is examined. For the investigation of uncertainties, a Monte-Carlo method is chosen to ensure statistically significant results. For the sake of comparability, reference cases using ground-based observations are carried out. In addition, sensor fusion cases are conducted by considering a combined usage of space- and ground-based data. Space- and ground-based observations as well as the orbits which are used for these studies are simulated. Moreover, sensor surveys are conducted using ESA's Program for Radar and Optical Observation Forecasting (PROOF) software tool to analyze detection capabilities of a space-based sensor. Objects detected during the survey are used for follow-up observation campaigns, re-visiting and actively tracking the same targets to enhance estimation accuracy. Both surveys and follow-up campaigns are conducted for different orbital regimes, taking into account the respective catalogued population. For these studies, telescope and sensor specifications as well as mission constraints are based on a currently operational space-based sensor.

Keywords: Space-based sensors; optical observations; orbit determination; Space Surveillance and Tracking.

## 1. INTRODUCTION

Currently, Space Surveillance and Tracking (SST) telescopes almost exclusively operate from Earth's surface, which has the disadvantage that observation capabilities are limited by geometrical and viewing constraints. Particularly the dependency on cloudless skies as well as favorable seeing conditions, limits sensor availability for

ground-based telescopes. An approach to overcome these limiting factors is the usage of space-based telescopes. Space-based observations are not constrained by the atmosphere, day or night time, weather conditions and geographical location.

Over the past 20 years, several space-based telescopes have been launched and demonstrated the feasibility of the technology for space debris observations. Currently, observations obtained by some of these missions, such as the Geosynchronous Space Situational Awareness Program (GSSAP), contribute to the Space Surveillance Network (SSN) [6]. However, to define future missions, the influence of different observation conditions and requirements, compared to conventional ground-based observations, must be understood and quantified. The viability and field of application of such a system is impacted by various parameters, such as the orbit of the observer, the orbital regime to be observed, the observation strategy, the sensor and telescope specifications as well as constraints of the satellite itself. While all of these contributing parameters must be considered when developing future systems, many aspects have not been sufficiently studied. With the aim to contribute to closing this knowledge gap, this work investigates the potential of space-based optical observations for orbit determination (OD) and examines achievable estimation accuracies.

Estimation accuracy directly depends on uncertainties and biases affecting the measurements. Therefore, particular attention is paid to the investigation of uncertainties such as measurement noise and position errors of the observing satellite and their impact on the estimation performance. For that purpose, assumptions for the observation geometry and sensor specifications are made based on currently operational and potential future missions. In order to put the obtained results into perspective, additional cases using ground-based observations are considered and compared to the space-based cases. Further, orbit determination is conducted with a combined usage of ground- and space-based data, also known as sensor fusion.

Since all orbital regimes are affected by space debris, they must all be observed to achieve full coverage of the space population. However, due to various distances, rel-

ative velocities and illumination conditions for different orbits, sensor and telescope requirements deviate as well. Currently operational systems are therefore designed to obtain measurements of specific orbits rather than covering the whole orbital population. Due to the fact that only a few space-based sensors have been deployed, capabilities and corresponding requirements have not been defined for all sensor configurations and relative geometries. Moreover, extensive mission specifications and observation data obtained by these systems is typically not publicly available, which further widens the knowledge gap. In order to investigate observation capabilities of a space-based sensor and to contribute defining orbit specific requirements, observation campaigns are simulated for different orbital regimes. These campaigns are conducted for low Earth orbits (LEO), geostationary orbits (GEO) as well as highly elliptical orbits (HEO), while considering the respective populations by using a current TLE catalog procured from [10]. Sensor and mission constraints of a currently operational space-based system are considered to represent a scenario as realistic as possible. Finally, the influence of varying sensor specifications on observation capabilities is examined.

The following studies and associated results, are based on a Master thesis [11] conducted in cooperation between GMV and the Technical University of Darmstadt.

## 2. SIMULATION PROCEDURE

All data utilized in this work has been simulated using GMV's flight dynamics software library. Figure 1 outlines the procedure to simulate orbits as well as observations. First, initial state vectors for the observer and target object are used to simulate reference orbits serving as ground-truth. That is done by propagating high fidelity perturbation models using a numerical integrator, considering forces such as solar radiation pressure, non-spherical gravity field of the Earth, atmospheric drag and third-body perturbations. Table 1 lists the considered perturbation forces of the dynamical model. Then, the obtained orbits are utilized to simulate space-based measurements, while taking measurement noise into account.

Table 1. Perturbation force models considered for propagation

Perturbation	Model
Earth Gravity Potential	EIGEN-GRGS-RL04
Atmospheric Density Model	NRLMSISE-00
Third Body Perturbations	DE440
Solar Radiation Pressure	Cannonball Model

The resulting observations can then be used in the orbit determination procedure, which is described in detail in

[15] and [7]. The estimation is performed using the non-linear weighted least squares method, which minimizes the squares of the residuals  $R$ , i.e. the following loss function  $J(x_0)$ .

$$J(x_0) = R^T \cdot W \cdot R = (y - y_g)^T W (y - y_g) \quad (1)$$

Where  $W$  denotes the weighting matrix which considers observation errors,  $x_0$  the initial state,  $y$  the actual measurements and  $y_g$  reconstructed measurements. In order to compute the reconstructed observations, the initial state as well as the reference orbit of the observer must be provided. The loss function minimization for GEO objects was performed using the Gauss-Newton method. Since convergence of LEO and HEO estimations was found to be more sensitive to poor a-priori information, a more robust Levenberg-Marquardt algorithm was chosen, due to its larger radius of convergence [5]. Due to the high non-linearity of the underlying dynamical model, a linearization around the initial state is performed. With the aid of the Jacobian matrix  $H$ , containing the partial derivatives, the corrections  $\Delta x$  can be determined.

$$\Delta x = (H^T \cdot W \cdot H)^{-1} \cdot H^T \cdot W \cdot R \quad (2)$$

The obtained corrections  $\Delta x$  are then used to refine the initial state  $x_0$ . The updated state  $x_1$  serves as a new initial guess for the next iteration.

$$x_1 = x_0 + \Delta x \quad (3)$$

That process is repeated until the solution converges and additional iterations yield no improvement. After convergence of the loss function minimization, the resulting estimated state is compared to the ground-truth. Deviations between estimated and true state are then analyzed regarding uncertainties and considered observation conditions.

## 3. UNCERTAINTY INVESTIGATION

The same observational setup is used for subsequent studies examining the effects of uncertainties on achievable estimation accuracy. The space-based telescope is located in a sun-synchronous orbit (SSO) and observes the target in GEO. Keplerian elements for both are listed in Table 2. In order to compare the estimation results obtained by using space-based observations, two additional ground-based telescopes have been considered. One of these telescopes is located in Tenerife, Spain and the other one in Yarragadee, Australia. For the sake of comparability, space- and ground-based observation campaigns have been configured as similar as possible. Particularly the number of observation arcs and their individual length determine the achievable estimation accuracy.

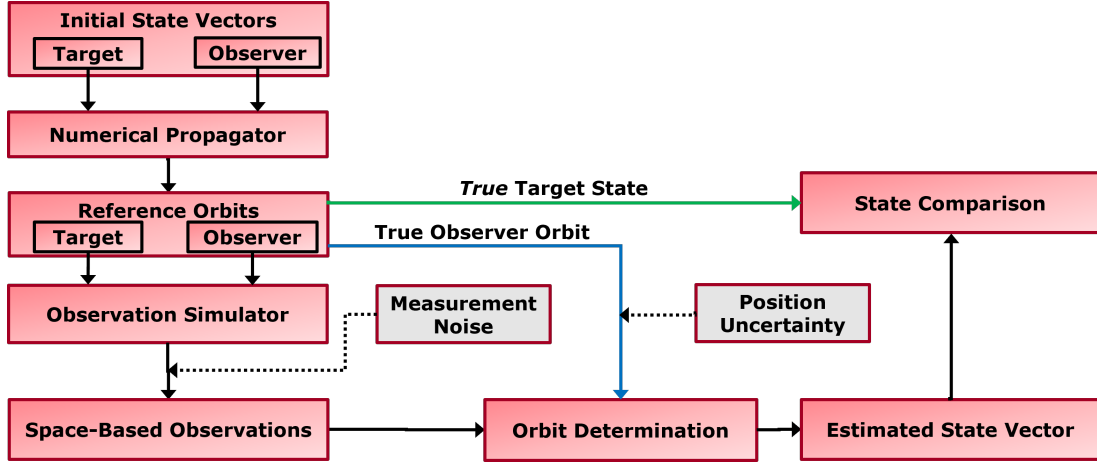


Figure 1. Simulation procedure to generate space-based observations, propagate reference orbits and conduct OD.

Therefore, the same amount of observations  $n_{obs}$  has been used for all cases, i.e.  $n_{obs,ground} = n_{obs,space} = n_{obs,fusion}$ . Each of the ground-based telescopes observed the target twice per night, which adds up to a total number of 16 tracks for the whole 8 day observation campaign. Accordingly, the space-based sensor re-visited the target four times each day, which can only be achieved when observations are also obtained when phase angles are not optimal. Further, each observation arc was set to be 3 minutes long, with an exposure repetition time of 10 seconds, i.e. each track consists of 18 individual measurements.

Table 2. Orbital parameters of the observer satellite and the observed target object

	Target object	Space-based telescope
$a$	42166 km	7180 km
$e$	0.0018584	0.0000963
$i$	1.6135°	98.6316°
$\Omega$	91.2765°	314.7528°
$\omega$	184.3406°	91.8064°

In order to cover objects which are either less frequently updated or where only IOD solutions are available, a more conservative approach regarding a-priori information has been chosen. Therefore a total a-priori error of about 8 km in position and 80 m/s in velocity has been applied.

Then measurement noise is computed by randomly generating values following a Gaussian distribution with zero mean and a standard deviation  $\sigma$ . Noise for right ascension and declination is assumed to be uncorrelated and has equal standard deviations  $\sigma_{RA} = \sigma_{Dec}$ . Computed measurement noise  $n_i$  is then added to the simulated measurements  $y(t_i, r_i)$ .

$$\tilde{y}(t_i, r_i) = y(t_i, r_i) + n_i \quad (4)$$

Similarly to the measurement noise computation, position uncertainty of the observer is introduced by generating a normally distributed random error with zero mean and a standard deviation  $\sigma_{pos}$ . Subsequently, these errors  $\delta_{pos,i}$  are added to the true state vectors of the observer satellite  $\vec{r}(t_i)$ .

$$\tilde{\vec{r}}(t_i) = \vec{r}(t_i) + \delta_{pos,i} \quad (5)$$

In order to minimize the influence of randomness and quantify the impact of the uncertainties  $n_i$  and  $\delta_{pos,i}$  on estimation accuracy, Monte-Carlo simulations have been used for both studies.

### 3.1. Impact of Measurement Noise

Figure 2 depicts the total root mean squares error (RMS) at the estimation epoch for measurement noise levels from  $\sigma = 0.3$  mdeg up to  $\sigma = 3.0$  mdeg. Total position RMS was computed according to

$$RMS_{total} = \sqrt{RMS(T)^2 + RMS(N)^2 + RMS(W)^2}. \quad (6)$$

Where  $RMS(T)$ ,  $RMS(N)$  and  $RMS(W)$  are the RMS errors in each direction of the local satellite frame. The T-axis is defined to point in the direction of the velocity vector and the N-axis is perpendicular to the velocity, where both T and N lie in the orbital plane. The W-axis on the other hand points in the direction of the angular momentum and is therefore perpendicular to the orbital plane. For the following investigations of GEO, orbits are nearly circular with eccentricities  $e \approx 0$ , thus the N-axis is referred to as the radial direction. The RMS error in the along-track direction is determined by

$$RMS(T) = \sqrt{\frac{\sum_{j=1}^n \Delta T(t_i)_j^2}{n}} \quad (7)$$

and can be computed analogously for the radial and cross-track direction. Here,  $j$  corresponds to a single Monte-Carlo simulation and  $i$  to a certain epoch. For the following investigation  $n = 100$  is assumed, thus each of the three displayed cases represents the RMS of one hundred Monte-Carlo simulations. It can be seen that increasing noise leads to a nearly linear increase in RMS for the ground-based, space-based and sensor fusion case. The lowest total position RMS i.e. the best overall estimation performance was observed when using ground-based observations exclusively. Particularly, for noise levels above  $\sigma = 1$  mdeg the total RMS is up to 10 percent lower compared to the space-based and sensor fusion case.

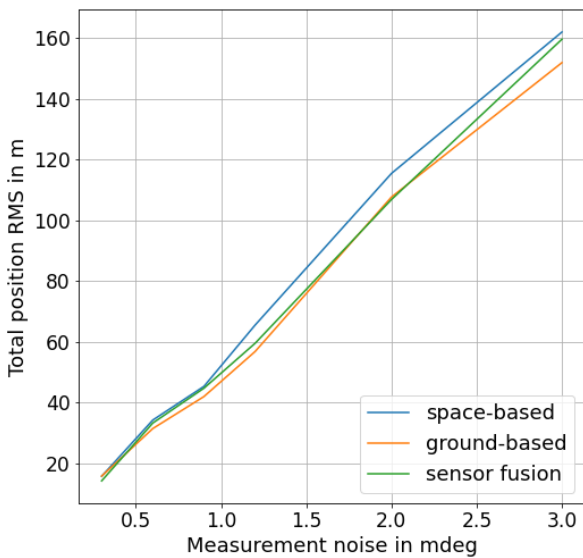


Figure 2. Total RMS error after OD as a function of measurement noise for space-based, ground-based and combined observations

The origin of deviating performances can be explained by comparing the position RMS of each directional component separately. Figure 3 depicts the estimation of each directional component in the local frame relative to the ground-based case. More specifically, values for space-based and sensor fusion above zero represent a reduction of the estimation error with respect to the ground-based case. Utilizing solely space-based observations leads to a decline of around 10 to 20 percent estimation accuracy in the along-track direction depending on the noise level. Estimation of the along-track component is particularly accurate for ground-based sensors due to the almost stationary relative geometry between observer and target. The relative motion of the target object primarily takes place in the plane of observation. Therefore, obtaining additional measurements particularly improved the estimation in along- and cross-track direction. While im-

provement of the radial component perpendicular to the observed plane was significantly lower. The performance in the radial direction on the other hand, is improved in a similar order of up to 20 percent when using space-based data. That behavior can be explained by the increased parallax due to the large and variable distance of the observer from the orbital plane of the target object. The observer orbit has a semi-major axis of  $a = 7180$  km and an inclination of  $i = 98.61$  deg. That means the observer oscillates between a distance of over 7000km below and above the orbital plane of the target during its orbital period of  $T \approx 100$  min. Whereas for the ground-based observer the distance to the orbital plane and the target itself, is nearly constant and directly depends on the latitude of the observatory.

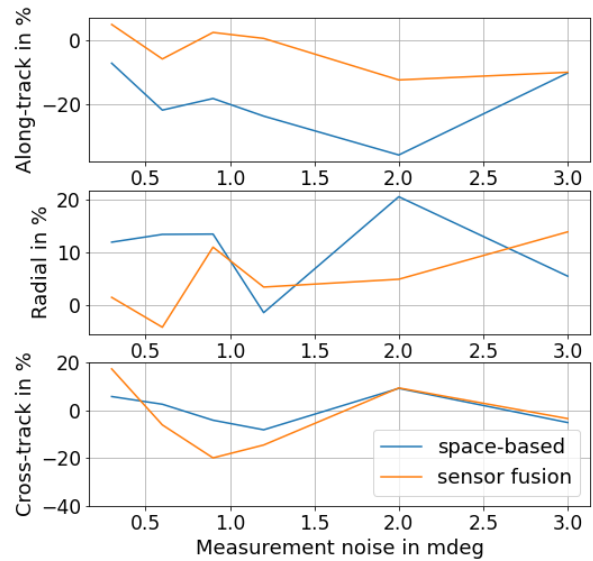


Figure 3. Relative error with respect to OD using only ground-based data. Positive values denote reduction of total RMS errors compared to the ground-base case in percent

While results fluctuate depending on the considered noise level, a clear trend for both along-track and radial direction could be observed. For the cross-track direction on the other hand no distinct trend could be observed. It must be noted that for all cases the same number of observations was used which explains why performance deteriorates in some cases when both space- and ground-based data is used in sensor fusion. In these cases less accurate along-track estimation performance of the space-based data reduced overall estimation performance.

These results can be put into perspective when comparing the noise levels investigated to the ones of an operational space-based sensor system. NEOSat for example has an average measurement noise of  $\sigma = 2.88'' \approx 0.8$  mdeg, when assuming observations of the GEO belt [1]. Applying measurement noise of that order here, leads to a total position RMS of below 50 m at the estimation epoch. Currently achievable estimation accuracies for a

space-based sensor are therefore well below the required cataloguing requirements of 100 m position uncertainty [8]. Further, it can be seen that even noise levels up to  $\sigma \approx 1.7\text{mdeg}$  can be sustained, while satisfying the 100 m threshold required for cataloguing. However, future missions are anticipated to have significantly lower astrometric noise in the order of  $\sigma = 1'' \approx 0.28\text{mdeg}$  [14] [3]. Thus, they have the potential to reduce estimation errors by 50 percent with respect to current systems.

### 3.2. Impact of Position Uncertainty of the Observer

To evaluate the influence of each directional error on the estimated state isolated, position uncertainties of the observer were tested in along-track, radial and cross-track direction separately. Further, to isolate the effect of position errors and decouple two normally distributed parameters, measurement noise was only generated once and scaled for this investigation. Figure 4 depicts the resulting position RMS after the OD when varying both measurement noise and observer position uncertainty in along-track direction. Each field displayed in the heat map represents the outcome of 50 Monte-Carlo simulations for a certain combination of measurement noise and position uncertainty. When considering low but realistic noise of  $\sigma = 0.3\text{mdeg}$  or above, position errors up to 10 m have negligible effect on obtained RMS errors. It can be seen that the influence of position uncertainty on the overall error degrades with increasing noise. Thus, sensor systems with low astrometric accuracies can sustain higher position uncertainties without sacrificing estimation accuracy.

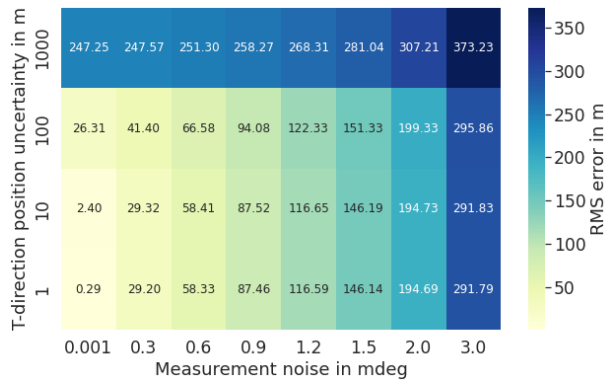


Figure 4. Total RMS error at the estimation epoch as a function of measurement noise and position uncertainty of the observer in along-track direction

The following Figures 5 and 6 depict the resulting position RMS, when varying both measurement noise as well as observer position uncertainty in radial and cross-track direction respectively. Due to the fact that measurement noise dominates the overall error for position uncertainties of 10 m and below, RMS errors are almost identical, regardless of the direction of the uncertainty. Uncertainties in along-track and radial direction yield very similar

RMS errors, only deviating by up to 5 percent. However, estimation was found to be more robust regarding errors in cross-track direction, particularly for higher noise levels. When considering noise of  $\sigma = 0.6\text{mdeg}$  and above, position uncertainties in the radial and along-track direction of 100 m lead to an increase in RMS errors of up to 14 percent. Applying the same uncertainty in the cross-track direction yields an increase of RMS errors of below 4 percent.

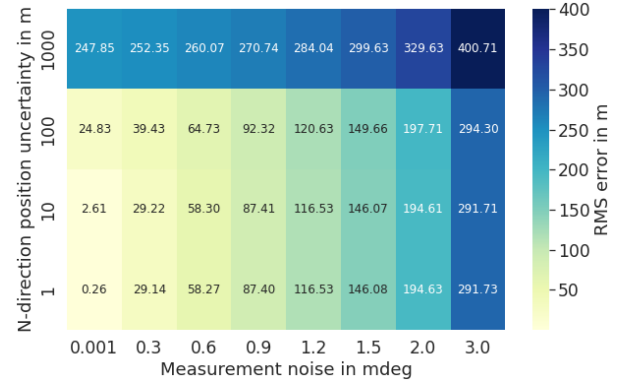


Figure 5. Total RMS error at the estimation epoch as a function of measurement noise and position uncertainty of the observer in radial direction

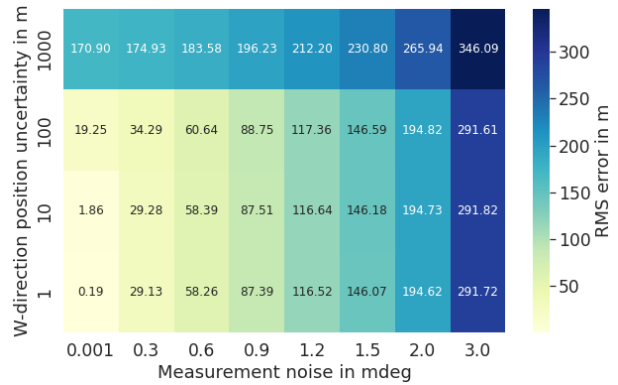


Figure 6. Total RMS error at the estimation epoch as a function of measurement noise and position uncertainty of the observer in cross-track direction

As mentioned earlier, currently operational sensor systems such as NEOSat, have an expected noise between  $\sigma = 0.8\text{mdeg}$  and  $\sigma = 1.2\text{mdeg}$  depending on observation conditions. Therefore, position uncertainties in either direction up to 10 m have insignificant impact on estimation accuracy. Errors in the order of 100 m in along-track or radial direction can be sustained while increasing position RMS up to 10 percent. In cross-track direction, even 100 m errors only increase position RMS by about 2 percent. Further, it can be seen that required accuracies for cataloguing can be satisfied even with position uncertainties of 100 m in either direction, as long as measurement noise is below 0.9 mdeg. However, planned sensor

systems with considerably lower astrometric noise in the range of 1'' are much more sensitive to position uncertainties. For errors of 100 m in along-track or radial direction, an increased RMS of up to 40 percent can be expected.

#### 4. SURVEYS AND FOLLOW-UP CAMPAIGNS

The following study examines detection as well as tracking capabilities of a space-based sensor under realistic conditions. First, ESA's Program for Radar and Optical Observation Forecasting (PROOF) has been used to conduct sensor surveys for different orbital regimes. Here, a space-based sensor has been modeled based on NEOSSat's telescope and sensor specifications listed in Table 3. During these surveys the telescope is pointing in a fixed inertial direction and detects objects crossing its field of view (FOV). Here, a recent Two Line Element (TLE) catalogue representing the real orbital population has been used. That catalogue was retrieved from [10] and entails over 25000 objects.

Table 3. NEOSSat telescope configuration and CCD sensor specifications considered for the simulated surveys, from [12] and [13]

Telescope	Maksutov-Cassegrain
Aperture Diameter	157 mm
Focal Ratio	$f/6$
FOV	$0.85^\circ \times 0.85^\circ$
Sensor Resolution	$1024 \times 1024$ pixel
Pixel Size	$13 \mu\text{m}$
Spatial Resolution	$3''/\text{pixel}$
Peak Quantum Efficiency	0.78
CCD Read Noise	11 e-/pixel
Dark Current (at 253K)	1 e-/s/pixel

Subsequently, detections made during the survey were used for a seven day observation campaign re-visiting and actively tracking these objects. However, restrictions such as the maximum slewing rate of the telescope or highest tolerable phase angles prevent the satellite from following some objects. To take those limiting mission constraints into account, objects previously detected during the survey, were filtered by angular velocity, apparent magnitude, signal-to-noise ratio (SNR) and phase angle. The limits chosen are based on NEOSSat and are listed in Table 4. To examine the extend to which these restrictions affect the ability to track the population, variations of the constraints have been tested. Objects fulfilling the mission constraints pass the filters and are therefore trackable by the sensor. These objects are then re-visited and tracked during the follow-up campaign whenever unobstructed visibility allows it. Obtained observations are then used for OD and estimated states are compared to the ground-truth.

Table 4. Mission constraints of NEOSSat considered for the follow-up observation campaigns, based on [1] and [13]

	Threshold
Angular velocity	$\omega \leq 215 \frac{\text{arcsec}}{\text{s}}$
Magnitude	$m \leq 15$
Phase angle	$\theta \leq 135 \text{ deg}$
Signal-to-Noise Ratio	$SNR \geq 3$

To evaluate the influence of both sensor and mission related constraints on the number of trackable objects, filters of different limiting parameters have been applied. Figures 7 and 8 depict tracking capabilities considering different constraints in angular velocity and apparent magnitude respectively. Only a single parameter is varied for each of the presented plots while the rest remain constant. Here, sensor specifications and mission constraints listed in Table 4 serve as the basis. For this overview no distinction between orbital regimes has been made, detections therefore correspond to all detectable objects of a current TLE catalogue. Duplicates, i.e. repeated detections of the same objects, have been eliminated. Figure 7 depicts the number of trackable objects as a function of the survey duration and the executable slewing rate of the telescope. It can be seen that the number of trackable objects significantly increases when higher slewing rates are permitted. Especially for observations in LEO, very high angular velocities occur, which in turn demand high slewing rates for LEO objects to be tracked.

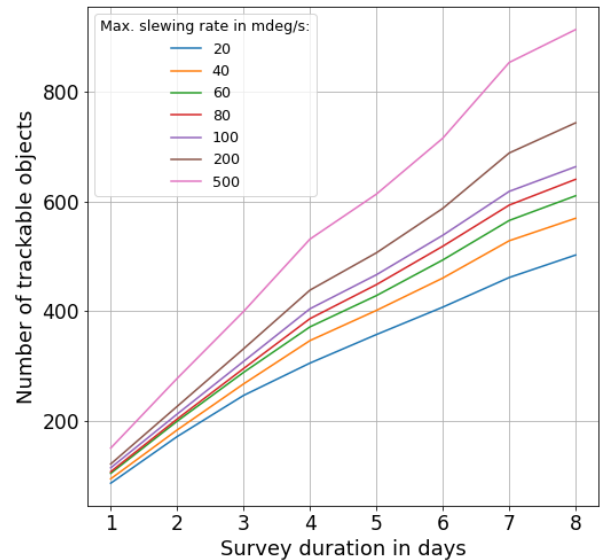


Figure 7. Impact of maximum permitted slewing rates of the telescope on number of trackable objects for different survey durations

Variations of the considered magnitude threshold for different survey durations is shown in Figure 8. At the assumed threshold of  $m \leq 15$  a saturation was observed, where only negligible improvements were achieved when increasing the magnitude threshold beyond  $m = 16$ . As mentioned before, detections considered here were obtained during a survey, which limits the sensor capability to concentrate light on a preferably small number of pixels. That means, at  $m \approx 16$  the sensors limiting magnitude is reached. However, if accurate a-priori information is available, the telescope can adjust its angular velocity to the one of the target, before actually detecting the object. Using that approach, enough light can be collected by a few pixels to raise the SNR and therefore successfully observe objects with higher magnitudes.

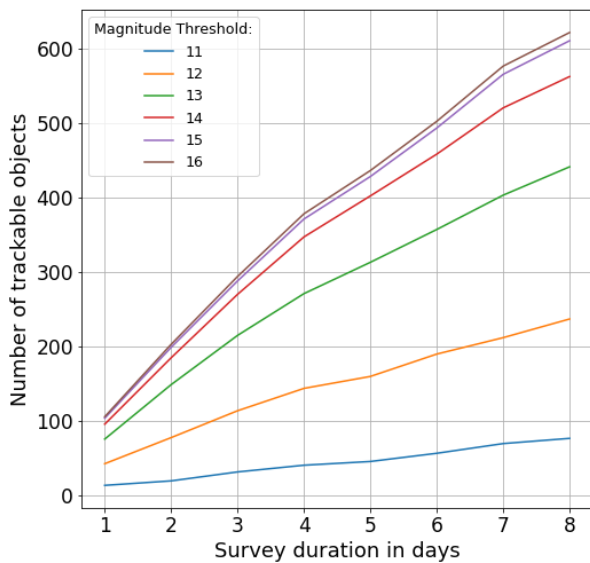


Figure 8. Impact of magnitude threshold on number of trackable objects for different survey durations

The surveys and observation campaigns discussed in the following sections are separated into three different classes: LEO, GEO and HEO. Here, each orbital regime is investigated with its corresponding assumptions, such as variations in the a-priori solution and measurement noise. However, for all observation campaigns only objects are considered and actively tracked which satisfy the constraints listed in Table 4. Furthermore, it is assumed that track-to-track association has already been performed. Therefore, it is always known which observation arcs belong to the same objects.

#### 4.1. LEO

During the seven day survey a total of 1224 LEO objects could be detected by the sensor, from which 101 were in line with the mission constraints and could therefore be actively tracked by the sensor. Thus, roughly 8 percent of detected LEO objects were considered in the tracking

campaign. Over 80 percent of the rejections were due to transgression of the angular velocity threshold, particularly for objects with low inclinations. The average angular velocity of detected LEO objects was found to be  $\omega \approx 0.17^\circ/s$ , thus almost three times the maximum slewing rate of the telescope. Another factor strongly affecting estimation accuracy and convergence is the assumed a-priori deviation from the ground-truth. Here, the a-priori knowledge is chosen with a total error of 1.8 km, with deviations from the ground-truth of 1.6 km in along-track direction and 0.6 km in cross-track and radial direction. The proportions of the directional uncertainties are based on [4], whereas their magnitude is assumed to be higher. The idea is to consider more conservative a-priori errors in order to cover objects which are either not catalogued yet or less frequently updated and therefore possess higher uncertainties. For observations in LEO a relatively high measurement noise of  $\sigma = 1.2$  mdeg was considered. That assumption of an elevated noise level was made due to the high slewing rates required to track objects in LEO. Increased tracking rates during the exposure lead to additional star elongation, which reduces achievable astrometric accuracy. The distribution of the total position RMS error for observed LEO objects is depicted in Figure 9. Due to the fact that 5 percent of objects have RMS errors above 1 km, the average RMS error was found to be 98 m. The median on the other hand is 16 m. Therefore, around 92 percent of objects satisfy accuracy requirements for LEO proposed by [2], with maximum errors of 200 m in along-track, 40 m in radial and 100 m in cross-track direction. Half of the remaining 8 percent of objects which are not suitable for cataloguing, meet the required total error of approximately 230 m. However, their range estimation yields errors above the 40 m threshold.

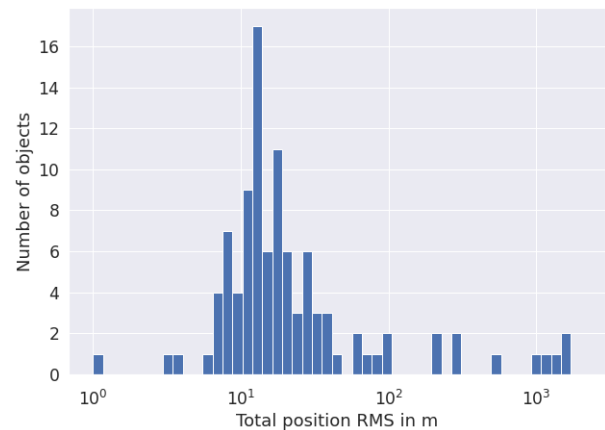


Figure 9. Total position RMS distribution for all tracked LEO objects

#### 4.2. HEO

During the simulated seven day survey of the HEO regime, 244 individual objects were detected. From those objects 89 satisfied all mission constraints and thus

could be actively tracked by the sensor. Similarly to the presented LEO survey, convergence proved to be extremely sensitive to errors of the a-priori solution. For the HEO observation campaign, a-priori knowledge is roughly based on estimated TLE accuracies [4]. The total error with respect to the true state is 1.9 km, with deviations of 1.3 km in along-track, 0.8 km in radial and 1.1 km in cross-track direction. Here, the same initial error is assumed for all HEO objects, regardless of influencing factors such as the individual eccentricity. Figure 10 depicts semi-major axis and eccentricity with corresponding position RMS errors after OD for all considered HEO objects. Here, no reduction of estimation accuracy could be observed with increasing eccentricity. It can be seen that many objects observed are located in geostationary transfer orbits (GTO) with an eccentricity of  $e \approx 0.73$  and a semi-major axis of  $a \approx 24500$  km. Deriving a-priori information for a GTO from TLEs yields errors several times higher than any other orbital regime [4]. Therefore, results for HEO, particularly those for GTO objects, cannot directly be compared to estimation errors found in the LEO and GEO campaigns where more conservative assumptions were applied. However, even with more favorable a-priori accuracy, than what could be expected in a real scenario, 10 percent of ODs failed due to divergence.

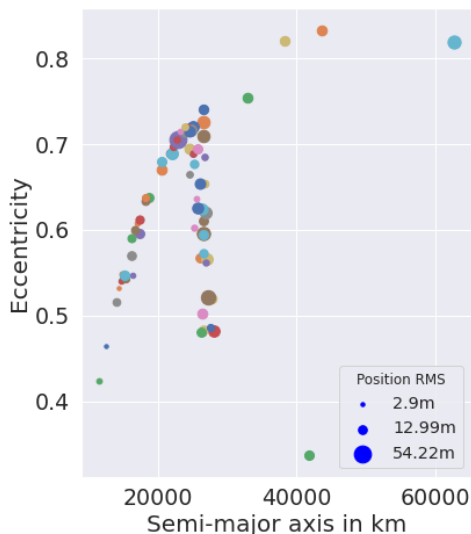


Figure 10. Semi-major axis and eccentricity of all tracked HEO objects and corresponding position RMS errors after OD

Figure 11 depicts the obtained RMS errors for all successfully determined orbits, while objects with failed estimations are excluded. The average RMS error achieved for the remaining objects is around 15 m, where all estimated orbits are in line with accuracy requirements for cataloguing. Due to the constraint in tracking rate, the vast majority of observations were made when the objects are closer to their apogee and as a result move slower with respect to the observer. Particularly objects with very high eccentricities move extremely fast close to their

perigee and therefore can not be tracked during that time when considering the angular velocity constraint. For that reason OD failure rate was relatively high, since many objects could not be re-visited frequently enough or the obtained tracks were very short due unfavorable viewing geometries. An approach to increase coverage could be accomplished by a combined usage of ground- and space-based sensors. Where radars observe the object at its perigee and follow-up measurements are made with a space-based sensor whenever the object is closer to its apogee and possesses considerably lower velocities.

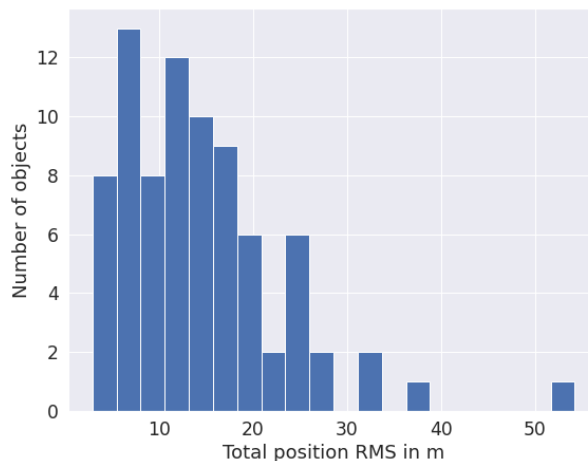


Figure 11. Total position RMS distribution for all tracked HEO objects

### 4.3. GEO

A total number of 483 individual objects was detected during the seven day survey, from which 221 fulfilled all mission constraints and thus could be tracked in the follow-up campaign. Compared to the tracking quota for LEO objects of below 10 percent, almost half of the detected objects can also be tracked in case of the GEO survey. Due to the large distance between observer and target, reflected light is becoming increasingly faint, the main limiting factor consequently is the apparent magnitude. During the survey objects up to magnitude  $m = 17$  could be detected, associated SNR values are however below the threshold of  $SNR = 3$ . Reducing the threshold significantly increases the number of detectable objects but the probability of spurious detections is increased as well. Incorrectly registered detections, not assignable to a real object are false-positives contaminating the catalogue and must be avoided. Alternatively, a larger aperture can be employed in order to enhance detectability of fainter objects during survey operations. Doubling the aperture quadruples the light collecting area of the telescope. Therefore, four times more photons can be captured by the sensor during the same exposure time. Surveys based on NEOSat's  $D = 15$  cm aperture were compared to a survey with identical configurations except  $D = 30$  cm aperture. It was shown that the number of

detected objects increased by around 40 percent. The additional detections predominantly correspond to objects with 1 m diameter and below. The lower size limit for detections of the smaller aperture is around 1.4 m, whereas for the larger one, objects of 0.8 m in size could be detected.

During the seven day observation campaign each target was re-visited three times per day on average, where almost half of the detected objects in GEO could be actively tracked by the space-based sensor. The exact number of tracks is object specific and depends on the particular visibility conditions. Theoretically, up to 75 percent of a GEO object's orbit could be tracked due to the high tolerable phase angle of  $\theta = 135^\circ$  [9]. However, to ensure better illumination conditions, all observations considered for OD were obtained with phase angles  $\theta \leq 90^\circ$ . Additionally, maximum track lengths of 3 minutes were permitted if unobstructed visibility allowed it. Due to the lower slewing rates required for GEO observations, astrometric noise of  $\sigma = 0.8$  mdeg has been considered.

Figure 12 depicts the obtained position RMS errors for all GEO objects which have been tracked. The average RMS error was found to be around 30 m. In direct comparison to the estimation accuracies shown for the LEO cases, errors appear to be relatively high, especially since observation arcs are considerably longer for the GEO campaign. However, it must be noted that given a-priori deviations are assumed to be significantly higher for the GEO case. The total deviation of the a-priori state from the ground-truth was assumed to be 5.7 km for each object, with 4.3 km in along-track, 3.6 km in radial and 0.9 km in cross-track direction. That assumption was feasible since convergence proved to be very robust with respect to high a-priori errors. Even extreme cases of more than 20 km total position deviation from the true state lead to convergence at a reasonable accuracy. From that it can be concluded, that even poor a-priori information derived from IOD or scarcely updated TLEs can be sufficient for a successful OD.

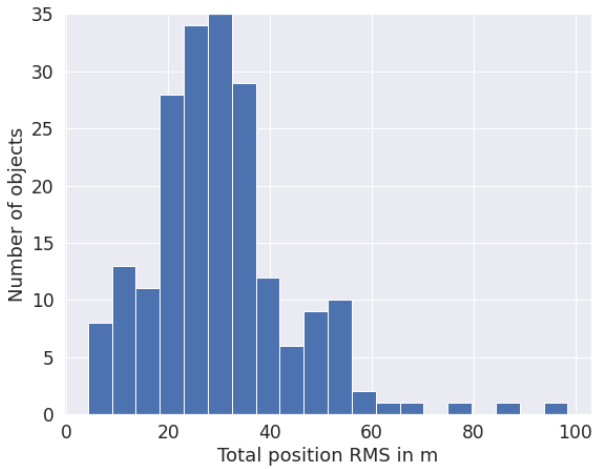


Figure 12. Total position RMS distribution for all tracked GEO objects; Average number of tracks per day  $n_{tr} \approx 3$

Since each object was re-visited three times per day on average, the total number of tracks considered for OD was therefore more than 20 on average. In real scenarios that assumption might not always be viable due to unfavorable illumination or conflicting sensor scheduling. To investigate the impact of fewer tracks considered for the OD procedure on achievable estimation accuracy, an additional case has been conducted, where one quarter of all available observations was used. Here, every fourth track, i.e. an average of  $n_{tr} \approx 0.75$  tracks per day was considered. The obtained RMS errors for that case are depicted in Figure 13. The average RMS was found to be around 54 m, which translates to an increase of 80 percent with respect to the reference case with  $n_{tr} \approx 3$ . Estimation for ten objects did not satisfy the cataloguing requirements of 100 m total error [8]. Nevertheless, over 95 percent of estimated orbital states were in line with the requirements, even when less than a track per day was considered. Therefore, it can be concluded that estimation for cataloguing services is feasible even when significantly fewer observations are available.

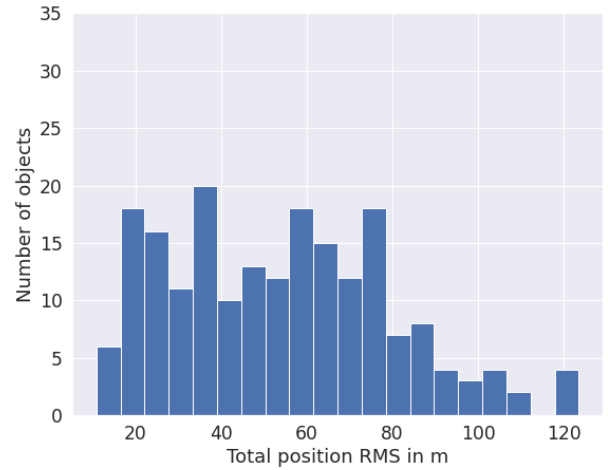


Figure 13. Total position RMS distribution for all tracked GEO objects; Average number of tracks per day  $n_{tr} \approx 0.75$

## 5. CONCLUSION

While overall estimation performance was found to be superior when using solely ground-based data for GEO observations, space-based measurements yielded significant improvement in range estimation. It was shown that measurement noise up to  $\sigma = 6'' \approx 1.7$  mdeg can be tolerated while fulfilling cataloguing requirements of up to 100 m total position errors. These results were obtained based on the conservative assumption of poor a-priori knowledge, with deviations from the true state an order of magnitude larger than what can be expected from TLEs. Additionally, conducting ODs with considerably fewer observations showed that cataloguing requirements can be fulfilled. Thus, estimation for GEO objects proved to be very robust regarding poor initial information as well as

shortage of measurement data.

It must be emphasized again that a significantly higher sensor availability of a space-based system is of great value for cataloguing activities. The considered system enabled reliable observations at least once a day, regardless of weather or other restrictions which might prevent sufficient tracking from ground. However, in order to further enhance coverage and track smaller objects, larger apertures must be employed. It was found that the number of detectable objects increases by around 40 percent when doubling the aperture to  $D = 30$  cm.

Furthermore, it was shown that position errors of the observer in either direction of up to 10 m have a negligible effect on estimation accuracy. The extend to which position errors affect the estimated states is directly linked to the assumed noise level. While higher position uncertainties degrade the achievable estimation accuracy, cataloguing requirements can be satisfied for position uncertainties up to 100 m, if present noise levels are below  $\sigma \approx 0.9$  mdeg.

Observation and subsequent state estimation for objects located in LEO and HEO proved to be more challenging compared to GEO. Firstly, due to different shapes and orientations of the orbital planes as well as distances between observer and target, observation geometries vary strongly. Secondly, estimation procedure and its convergence is very sensitive to poor a-priori information. In order to improve coverage and re-visit objects more frequently, high tolerable phase angles must be facilitated. That can be achieved by using a baffle, enabling the sensor to observe within low solar elongations. Further, to ensure longer observation arcs and track objects in closer proximity, high slewing rates of the telescope are required. However, to accomplish that, capable attitude determination and control systems must be employed, which increases complexity and costs of the system.

## 6. FUTURE WORK

A multitude of parameters related to the sensor, telescope optics, observation strategy and the satellite itself determine the capabilities and field of application for a space-based sensor. Due to the fact that only a fraction of all possible parameter combinations could be investigated within the scope of this work, aspects which could not be covered but are of interest will be outlined in the following list.

- **Initial Orbit Determination (IOD):** Rather than considering a-priori information based on TLEs and expected IOD solutions from literature, as done in this work, the initial solution could be derived from space-based observation by IOD. Using that approach would represent a more realistic scenario.

- **Space-based sensor constellations:** Employing additional space-based sensors as a constellation could significantly shorten re-visiting periods and therefore increase achievable estimation accuracies.
- **Considering maneuvers:** Since maneuvers alter the orbital trajectory of a satellite, they potentially degrade the quality of available a-priori information, make re-visiting the object more difficult and impact the estimation accuracy. Therefore, maneuvers must be considered for a more realistic scenario when functional satellites are observed.
- **Observations of fragmentation events:** Observations shortly after break-up or fragmentation events could be beneficial using a space-based sensor. Due to the fact that objects are in close proximity and measurements are unaffected by the atmosphere, smaller objects might be observable compared to a ground-based sensor.

## ACKNOWLEDGMENTS

The presented work, with all its investigations and associated results, is based on a Master thesis [11] conducted in cooperation between GMV and the Technical University of Darmstadt.

## REFERENCES

1. Abbasi, Viqar, Stefan Thorsteinson, David Balam, Jason Rowe, and Robert Scott (2019). "The NEOSat Experience: 5 years in the life of Canada's space surveillance telescope".
2. ESA (2013). Space Situational Awareness - Space Surveillance and Tracking System Requirements Document.
3. Flohrer, Tim, Holger Krag, H. Klinkrad, and T. Schildknecht (2011). "Feasibility of performing space surveillance tasks with a proposed space-based optical architecture". In: *Advances in Space Research* 47. issn: 02731177. doi: 10.1016/j.asr.2010.11.021.
4. Flohrer, Tim, Holger Krag, H. Klinkrad, Benjamin Virgili, and Carolin Frueh (2009). "Improving ESA's Collision Risk Estimates by an Assessment of the TLE orbit Errors of the US SSN Catalogue"
5. Gavin, Henri (2022). "The Levenberg-Marquardt algorithm for nonlinear least squares curve-fitting problems".
6. Gilmore, Micheal (2016). Director, Operational Test and Evaluation - Annual Report 2016. url: <https://www.dote.osd.mil/Portals/97/pub/reports/FY2016/other/2016DOTEAnnualReport.pdf?ver=2019-08-22-105134-547>.
7. Montenbruck, Oliver and Eberhard Gill (2000). *Satellite Orbits: Models, Methods and Applications*. Berlin, Heidelberg: Springer Berlin Heidelberg. isbn: 978-3-642-58351-3.

8. Naka, F.R., G.h. Canavan, R.A. Clinton, and O.P. Judd (1997). "Space Surveillance, Asteroids and Comets, and Space Debris." In: Volume 1: Space Surveillance.
9. Scott, Robert and Stefan Thorsteinson (2018). "Key findings from the NEOSat space-based SSA microsatellite mission"
10. SpaceTrack (2022). Two Line Element Catalogue. url: <https://www.space-track.org> (visited on 11/02/2022).
11. Stechowsky, Felix (2023). "Orbit determination and correlation using space-based optical telescope observations". Master-Thesis. Technische Universität Darmstadt
12. Teledyne (2017). CCD47-20 Back Illuminated AIMO Frame-Transfer High Performance CCD Sensor. url: <http://www.e2v.com/resources/account/download-datasheet/1427>.
13. Thorsteinson, Stefan (2017). "Space Surveillance from a Microsatellite". Master-Thesis. Royal Military College of Canada.
14. Utzmann, Jens, Luis Ferreira, Gerard Vives, Lionel Métrailler, Nicolas Lièvre, and Tim Flohrer (2017). "Optical In-Situ Monitor – A Step towards European Space-Based Debris Observations"
15. Vallado, David A. and Wayne D. Mac Clain (C 2013). Fundamentals of astrodynamics and applications. 4th ed. Space technology library. Hawthorne (CA): Microcosm Press. isbn: 9781881883197.